minerals

MDPI

Article

Measurements of Thermodynamic Data of Water in Ca-Bentonite by Relative Humidity Method

Kosuke Ichikawa * and Haruo Sato

Graduate School of Environmental, Life, Natural Science and Technology, Okayama University, 3-1-1 Tsushima-naka, Kita-ku, Okayama City 700-8530, Okayama, Japan; sato.haruo@cc.okayama-u.ac.jp
* Correspondence: pe5u0rtq@s.okayama-u.ac.jp

Abstract: Buffer material (compacted bentonite), one of the engineered barrier elements in the geological disposal of a high-level radioactive waste, develops swelling stress due to groundwater penetration from the surrounding rock mass. Montmorillonite is the major clay mineral component of bentonite. Even previous studies provide few mechanical and thermodynamic data on Ca-montmorillonite. In this study, thermodynamic data on Ca-montmorillonite were obtained as a function of water content by measuring relative humidity (RH) and temperature. The activities of water and the relative partial molar Gibbs free energies of water were determined from the experimental results, and the swelling stress of Ca-bentonite was calculated using the thermodynamic model and compared with measured data. The activities of water and the relative partial molar Gibbs free energies obtained in the experiments decreased with decreasing water content in water contents lower than about 25%. This trend was similar to that of Na-montmorillonite. The swelling stress calculated based on the thermodynamic model was approximately 200 MPa at a montmorillonite partial density of 2.0 Mg/m^3 and approximately 10 MPa at a montmorillonite partial density of 1.4 Mg/m^3. The swelling stresses in the high-density region (around 2.0 Mg/m^3) were higher than that of Na-montmorillonite and were similar levels in the low-density region (around 1.5 Mg/m^3). Comparison with measured data showed the practicality of the thermodynamic model.

Keywords: geological disposal; buffer material; Ca-montmorillonite; bentonite; swelling stress

Citation: Ichikawa, K.; Sato, H. Measurements of Thermodynamic Data of Water in Ca-Bentonite by Relative Humidity Method. *Minerals* **2024**, *14*, 477. https://doi.org/10.3390/min14050477

Academic Editors: Gianfranco Ulian and Jianxi Zhu

Received: 16 February 2024
Revised: 12 April 2024
Accepted: 22 April 2024
Published: 30 April 2024

1. Introduction

Radioactive waste is generated due to the operation and maintenance of nuclear power plants, fuel reprocessing plants, fuel fabrication facilities, uranium enrichment facilities, and facilities in which radioisotopes (RIs) are used. Currently, most of the radioactive waste remains in storage. Furthermore, the amount of radioactive waste generated by the operation of nuclear power plants and other facilities continues to increase. Therefore, there is a need to dispose of radioactive waste as quickly as possible.

Figure 1 shows the classification of radioactive waste, examples of waste, and disposal methods. In Japan, radioactive waste is classified according to its radioactivity level and is divided into two main categories: Low-Level Radioactive Waste (LLW) and High-Level Radioactive Waste (HLW) [1].

A conceptual diagram of the geological disposal is shown in Figure 2. In Japan, the vitrified waste is the HLW. After 30 to 50 years of cooling, the vitrified waste will be disposed of with engineered barriers in excavated tunnels in a geological formation deeper than 300 m.

Next, geological disposal is explained. The safety of the geological disposal in Japan is ensured by a multiple barrier system, which is a combination of the engineered barrier system and geological barriers with various protective functions (natural barrier). The multiple barrier system consists of, from the inside, vitrified waste, overpack, buffer material, and host rock. The buffer material is a compacted mixture of bentonite (natural

clay) and silica sand. Geological disposal is a safe method for HLW in a geological formation deeper than 300 m, isolated from the human environment until the radioactivity level of the waste becomes sufficiently low.

Type of Waste			Waste Examples	Sources	Disposal Methods (Example)
Low-level radioactive waste	Power Plant Waste	Very low-level radioactive waste	Concrete, Metal from decommission	NPPs	Trench disposal
		Relatively low-level radioactive waste	Liquid waste, Filter, disposal(gloves.etc)		Disposal in concrete vault
		Relatively high-level radioactive waste	Control rod, Channel boxes		Intermediate depth disposal
	Uranium Waste		Consumables, Sludge, Waste equipment	Uranium enrichment & fuel fabrication plant	Intermediate depth disposal, Disposal in concrete vault disposal, Trench disposal, in some cases Geological disposal
	Radioactive waste containing TRans-Uranium		Fuel rod parts, Waste liquid, Filter	Reprocessing plant, MOX fabrication plant	Geological disposal, Intermediate depth disposal, Disposal in concrete vault
High-level radioactive waste			Vitrified waste	Reprocessing plant	**Geological disposal**

Figure 1. Types of radioactive waste.

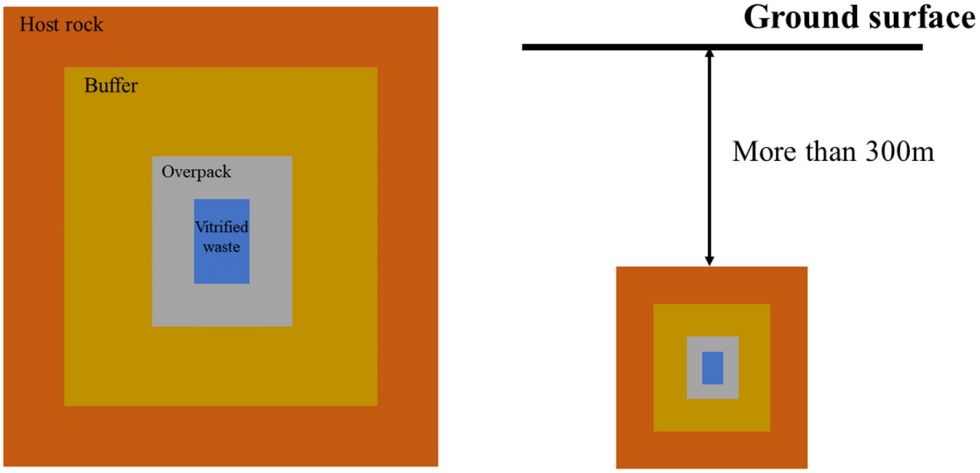

Figure 2. Overview of geological disposal (the **left** figure shows an overview of engineered barriers and the **right** figure shows an overview of geological disposal).

The bentonite being considered for use in Japan is a clay of which the main component is montmorillonite, a layered clay mineral, and Na-bentonite is planned to be used for geological disposal in Japan. It is also known that montmorillonite reflects the main physical properties of bentonite.

The properties of bentonite and montmorillonite are described below [2–4]. In the case of Kunigel V1 (produced by Kunimine Industries Co., Ltd., Tsukinuno, Yamagata Prefecture, Japan), which was used as a reference material in the reference case for the "Second Progress Report" [5] on the geological disposal of HLW, montmorillonite is contained in addition to chalcedony, plagioclase, calcite, dolomite, K-feldspar, and pyrite.

Figure 3 shows the crystal structure of montmorillonite, which is generally well known. The trivalent Al in the octahedral structure is partially replaced by divalent Mg and Fe. As a result, the crystal layer surface is charged with a negative permanent charge. Cations such as Na^+, Ca^{2+}, and K^+ ions exist between the aluminosilicate layers to compensate for the missing positive charge [2]. These cations are called exchangeable cations because they are easily exchanged with cations outside the interlayer. Those with Na^+ ions mainly in the interlayer are called Na-montmorillonite, and those with Ca^{2+} ions are called Ca-montmorillonite. Montmorillonite has a cation exchange capacity (CEC) of 100–110 meq/100 g, which is very high compared to other minerals. As shown in Figure 4, when montmorillonite comes in contact with water, water molecules selectively enter the interlayer by the hydration and solvation energies of the cations in the interlayer as the driving force, and this causes the interlayer to expand and swell. From the principle of swelling, the swelling property depends on the type of cations in the interlayer. When the volume of bentonite is constrained so that it does not swell, swelling stress (swelling pressure) is developed as a reaction force, and the mechanical buffering function is demonstrated by self-regulating water absorption and dehydration in response to external pressure [4].

Bentonite, primarily composed of the mineral montmorillonite, possesses notable properties including water sealing and self-sealing capabilities, mechanical buffering characteristics, and chemical buffering properties when exposed to aqueous environments. One of the specific events that may occur in an underground repository is that the overpack and vitrified waste may be subjected to mechanical stresses from the surrounding natural host rock, which may lead to premature failure of the overpack and vitrified waste. Specifically, the overpack is subjected to stress from the surrounding natural host rock, which is reported to have a mechanical strength of 10 to 35 MPa in Neogene sedimentary rock formations at a depth of about 500 m based on uniaxial compression test results [6,7]. Another report indicated values of 74–90 MPa for the Precambrian sedimentary rocks [7,8]. Thus, it is foreseeable that high pressures will be experienced during geological disposal. For these reasons, buffer and backfill materials are required to have mechanical and chemical buffering properties.

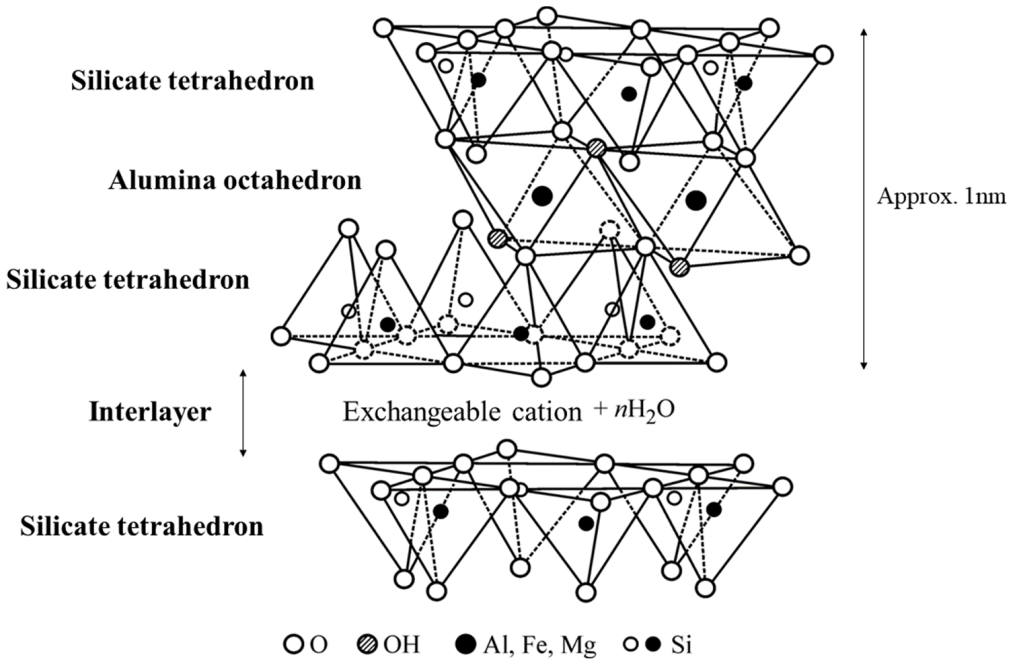

Figure 3. Crystal structure of montmorillonite [4] (partially modified).

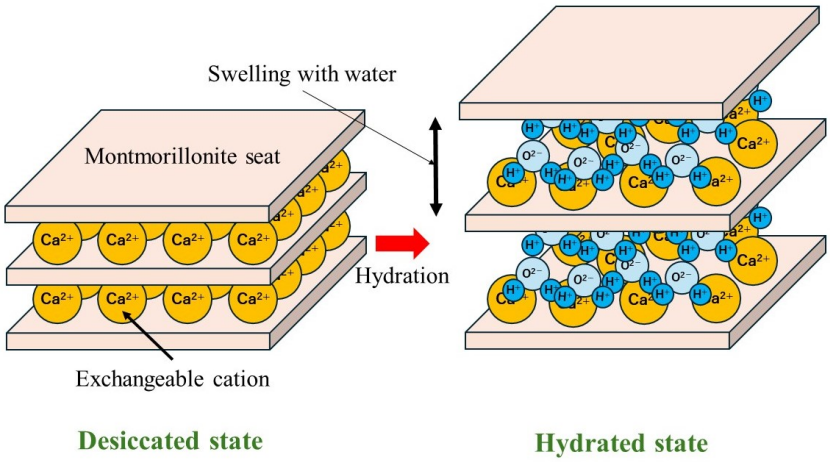

Figure 4. Montmorillonite swelling principle.

In 1992, the first progress report [9] was issued by the former Power Reactor and Nuclear Fuel Development Corporation (now the Japan Atomic Energy Agency, Ibaraki, Japan), which confirmed the technical feasibility of geological disposal in Japan. In 1999, the former Japan Nuclear Fuel Cycle Development Institute (JNC) reported the second progress report [5], which demonstrated the technical reliability and confirmed the technical feasibility of geological disposal in Japan.

Various data on bentonite, mainly on Na-bentonite such as Kunigel V1, which was used as a reference case in the second progress report, have been obtained for parameters such as dry density, silica sand content, and salt concentration, and have been published in the database of basic properties of buffer materials and in reports. The bentonite used for buffer and backfilled materials will be Na-bentonite, which is composed mainly of Na-montmorillonite. However, there is concern that Ca leaching from groundwater and concrete debris in the disposal tunnels may cause the interlayer cations of montmorillonite to be replaced by Ca^{2+} ions [10–13]. Since the swelling properties vary depending on the type of interlayer cations, the replacement of interlayer cations may prevent the buffer material from performing its expected functions.

Savage et al. [14] showed that during the post-closure period of a radioactive waste disposal facility, engineered barriers are saturated with groundwater, and cement-equilibrated pore fluids migrate to the surrounding host rock, suggesting that there may be geologic changes due to chemical reactions between the cement-equilibrated pore fluids and host rock that precede radionuclide migration. Kurosawa et al. [13] reported that montmorillonite altered to Ca-type in a saturated $Ca(OH)_2$ solution (pH about 12.5) simulating leachate from cementitious materials for Na-bentonite (Kunigel V1, 70% silica sand content). Kubo et al. [11] similarly confirmed that Na-montmorillonite was transformed to Ca-montmorillonite. Thus, it is quite possible that Na-bentonite could be altered to Ca-bentonite. Although some previous studies [9] have replaced Na-bentonite with Ca-bentonite and obtained swelling stress data, the data obtained were applicable only under limited conditions, making them less versatile. Gahr et al. [15] and Kanno et al. [16] predicted the relationship between swelling stress and the dry density of bentonite (Montigel, MX80, Kunigel V1) based on the moisture adsorption and desorption characteristics of bentonite. These studies suggest that it is useful to analyze the swelling stress of bentonite using models to confirm the safety assessment of radioactive waste disposal systems. However, the data used in the previous models are not generalizable because they can be applied only to individual bentonites.

Torikai [17] obtained thermodynamic data on water in compacted Na-bentonite, as elucidating the properties of water in montmorillonite is crucial. This is because radionuclides leached from vitrified waste diffuse through water to reach the buffer material. However,

the present study did not extend to calculating the swelling stress and comparing it with the measured data.

Sato [18,19] has developed a model to analyze swelling stress based on thermodynamic data and compared with measured data, but there are few results for other interlayer cations because the comparative results are mainly related to Na-montmorillonite.

As mentioned above, thermodynamic data on interlayer water in Ca-montmorillonite are almost non-existent and have not been discussed in detail, including uncertainties and reliability of thermodynamic data. The Na-bentonite that is planned to be used as a buffer material may be altered to Ca-bentonite due to leaching of Ca from groundwater or concrete materials during long-term isolation of high-level radioactive waste. Therefore, it is necessary to obtain a variety of data on bentonite with different interlayer cations to verify the safety of long-term radioactive waste disposal systems in detail.

In this study, we newly obtained thermodynamic data of water in Ca-montmorillonite, which does not exist also in the past studies, and calculated the swelling stress of bentonite using the thermodynamic model and compared with measured data to show the versatility and practicality of the thermodynamic model.

2. Thermodynamic Analysis of Swelling Stress

2.1. Thermodynamic Model for Swelling Stress

As explained above, water intrusion into the montmorillonite interlayer is a major factor in the swelling of bentonite. In other words, it is important to understand the behavior of interlayer water.

Among the parameters used in the thermodynamic analysis of swelling stress, we will first discuss water content, water activity, and relative partial molar Gibbs free energy. The water content is defined as the ratio of the mass of water to the mass of dry sample, as in Equation (1). The activity of water used in this study is defined as Equation (2). It is the degree of water binding in aqueous solution; that the activity of water is 1 stands for free water in the standard condition (25 °C), and that the activity of water 0 stands for structured water, where no free water is present. The activity of water takes values between 0 and 1. Let a_{H_2O} be the activity of the water, a_{H_2O} is defined by Equation (2). The relative partial molar Gibbs free energy of water can be obtained from Equation (3).

$$W_c = \frac{(M_s - M_d)}{M_d} \times 100 \quad (1)$$

$$a_{H_2O} = \frac{P_{H_2O}}{P^0_{H_2O}} \quad (2)$$

$$dG_{H_2O} = RT\ln\frac{P_{H_2O}}{P^0_{H_2O}} \quad (3)$$

W_c: Water content [%]
M_s: Mass of hydrated sample [g]
M_d: Mass of dried sample [g]
a_{H_2O}: The activity of water [-]
P_{H_2O}: Water vapor pressure [Pa]
$P^0_{H_2O}$: Vapor pressure of pure water at standard condition (25 °C) (=3.168 kPa) [Pa]
dG_{H_2O}: Relative partial molar Gibbs free energy [J/mol]
R: Gas constant [J/(mol·K)]
T: Absolute temperature [K]

Next, we will explain how to calculate the swelling stress of bentonite under pure water conditions. Figure 5 shows a conceptual diagram of the chemical potential balance when pure water (α phase) and bentonite (β phase) are in contact through a sintered metal filter and both phases are in equilibrium. The two phases are in contact through the filter, and the vapor pressure at the top reflects the state of water in the bentonite. The upper

spaces of the α and β phases are assumed to be completely independent. When water infiltrates from the α phase to the β phase and bentonite in the β phase is saturated, the chemical potentials of both phases become equivalent. At that time, the relative partial molar Gibbs free energy of water in the β phase changes, since water vapor pressure in the β phase increases by penetration of water from the α phase. In the absence of a filter at the top, the bentonite swells and works externally by increasing its volume, but in this case, the volume is constant, so the change in the relative partial molar Gibbs free energy of water acts as swelling energy.

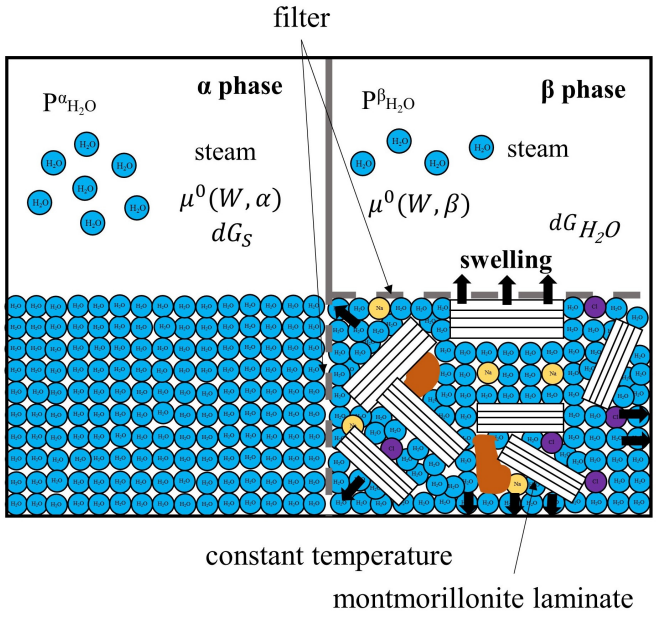

Figure 5. A conceptual model of the chemical potential balance of water in the equilibrium state between pure water (α phase) and water-saturated bentonite (β phase) through a sintered stainless steel filter at a constant temperature.

Since the activity of free water in Figure 5 is 1, the relative partial molar Gibbs free energy $dG_{H_2O} = 0$ from Equation (3). In the β phase, the relative partial molar Gibbs free energy of water changes as water infiltrates. When both phases are in equilibrium, the chemical potentials of water in both phases are equal, Equation (4) holds, and Equation (7) can be derived from Equations (5) and (6). In this case, the change in the relative molar Gibbs free energy of water in the β phase acts on the wall of filter as the swelling energy in Equation (8). The theoretical relationship between both phases is as follows.

$$\mu^0(W,\alpha) = \mu^0(W,\beta) \tag{4}$$

$$\mu^0(W,\alpha) = RT\ln\left(\frac{P^0_{H_2O}}{P^0_{H_2O}}\right) = 0 \tag{5}$$

$$\mu^0(W,\beta) = RT\ln\left(\frac{P_{H_2O}}{P^0_{H_2O}}\right) + \int_{P^0_{ext}}^{P_{ext}} V_{H_2O}dP \tag{6}$$

$$RT\ln\left(\frac{P_{H_2O}}{P^0_{H_2O}}\right) + \int_{P^0_{ext}}^{P_{ext}} V_{H_2O}dP = 0 \tag{7}$$

$$\int_{P^0_{ext}}^{P_{ext}} V_{H_2O}dP = -RT\ln\left(\frac{P_{H_2O}}{P^0_{H_2O}}\right) = -dG_{H_2O} \tag{8}$$

$\mu^0(W,\alpha)$: Chemical potential of α phase

$\mu^0(W, \beta)$: Chemical potential of β phase
P_{ext}, P^0_{ext}: Swelling stress when saturated with pure water and when dried [Pa]
V_{H_2O}: Molar volume of water (=18.0686, 25 °C) [cm^3/mol]

From Equation (8), assuming that the swelling stress of bentonite under dried condition is 0 and the volume of water is constant, Equation (9) is derived, and the swelling stress can be calculated from Equation (9).

$$dP_{ext} = -\frac{RT}{V_{H_2O}} \ln\left(\frac{P_{H_2O}}{P^0_{H_2O}}\right) = -\frac{dG_{H_2O}}{V_{H_2O}} \tag{9}$$

dP_{ext}: Swelling stress [Pa]

Next, montmorillonite partial density is described. As explained in this section, the swelling property of bentonite is due to volume expansion resulting from hydration of cations in the montmorillonite interlayer, and such properties of montmorillonite are reflected in the primary physical properties of bentonite. Therefore, it is considered optimal to normalize the swelling stress to montmorillonite partial density. Montmorillonite partial density is a parameter that focuses on the density of only the montmorillonite part in bentonite and is not necessarily the same as the dry density of bentonite, because bentonite includes montmorillonite and some other minerals as impurities. The montmorillonite partial density can be calculated from the bentonite dry density, silica sand content, particle density, and montmorillonite content using Equation (10) [20].

$$\rho_{dm} = \frac{(1 - f_s) f_m \rho_d}{1 - \left\{ \frac{(1-f_s)(1-f_m)}{\rho_{im}} + \frac{f_s}{\rho_s} \right\} \rho_d} \tag{10}$$

$\mu^0(W, \alpha)$: Chemical potential of α phase
$\mu^0(W, \beta)$: Chemical potential of β phase
P_{ext}, P^0_{ext}: Swelling stress when saturated with pure water and when dried [Pa]
V_{H_2O}: Molar volume of water (=18.0686, 25 °C) [cm^3/mol]
ρ_{dm}: Montmorillonite partial density [Mg/m^3]
ρ_d: Bentonite dry density [Mg/m^3]
ρ_{im}: Average true density of impurities (particle density) [Mg/m^3]
ρ_s: Silica sand true density (particle density) [Mg/m^3]
f_s: Silica sand content [-]
f_m: Montmorillonite content in bentonite [-]

Equation (10) is a formula for the dry density of bentonite, but because the experiments in this study were conducted as a function of water content, it is necessary to calculate the montmorillonite partial density in the water-saturated state. The conversion formula from water content is given by Equation (11).

$$\rho_{dm} = \left. \frac{100 \rho_{th} d_0}{W_c \rho_{th} + 100 d_0} \right|_{f_m = 1} \tag{11}$$

ρ_{th}: True density of montmorillonite (particle density) (=2.7 Mg/m^3) [Mg/m^3]
W_c: Water content [-]
d_0: Specific gravity of water under standard conditions (25 °C) (=0.997044)

In this study, temperature and relative humidity (RH) were measured using the relative humidity method. Therefore, the specific gravity of water used in Equation (11) was converted to match the measured temperature. Since the value of molar volume used in Equation (9) also changes, the molar volume at each temperature was obtained from the ratio of the specific gravity of water to the molar volume.

2.2. Substitutional Synthesis of Ca-Monimorillonite

Kunipia F (Kunimine Industries, Inc., Toyko, Japan montmorillonite content 99%), Na-bentonite, was used as the starting material in the substitution synthesis of Ca-montmorillonite. Table 1 shows the chemical compositions of Kunipia F for reference. The substitution process for exchangeable cations in the montmorillonite interlayer was based on the procedure of Sato et al. [20,21].

Table 1. Chemical composition of Kunipia F [22].

SiO_2	TiO_2	Al_2O_3	Fe_2O_3	MnO	MgO	CaO	Na_2O	K_2O	H_2O
58.0	0.2	21.9	1.9	0.2	3.4	0.5	3.0	0.1	10.8

Figure 6 shows a flowchart of the substitution synthesis of Ca-montmorillonite. The starting material, Kunipia F, was dried in a thermostatic oven (Yamato Scientific Co., Ltd., Tokyo, Japan) at 105 °C for several days and then weighed at 10.00 g using an electronic balance (AND Co., Ltd., Tokyo, Japan). The weighed bentonite and 500 mL of 1 M-$CaCl_2$ solution were placed in a triangular flask (500 mL) with a rotor at a liquid–solid ratio of 50 (mL/g) and stirred with a hot stirrer (Nisshin Rika Co., Ltd., Tokyo, Japan). The $CaCl_2$ solution was prepared using a special grade reagent (99.5% in purity) manufactured by Hayashi Pure Chemical Industry Co (Shiga, Japan). The stirred suspension was allowed to stand for approximately 1 week, after which the bentonite was immersed for 1 week, and solid–liquid separation was performed. When the suspension was allowed to stand, the bentonite was agglomerated and separated into two layers: a solid phase and a liquid phase. This is since when the salt concentration in the aqueous solution is high, the electric double layer on the montmorillonite surface becomes thinner and the interlayer cations become less hydrophobic (osmotic pressure decreases toward the outer layer), causing the bentonite to aggregate and settle at the bottom of the vessel. Solid–liquid separation was performed using this effect. After discarding the supernatant liquid of the suspension, which was separated into two layers, the supernatant near the boundary phase was carefully collected with a pipette. Next, 500 mL of a newly prepared 1 M-$CaCl_2$ solution was added and allowed to soak for approximately the same period, followed by solid–liquid separation in the same manner. This procedure was repeated three times.

After the third immersion, the supernatant liquid was discarded as much as possible, and the suspension was transferred equally into four centrifuge tubes for solid–liquid separation by centrifugation method. The final weight balance was adjusted by pipetting distilled water within 0.2 g. The centrifugation time was calculated from Stokes' law by the following equation.

$$t = \frac{63.0\eta \log_{10}\left(\frac{R}{S}\right)}{N^2(\sigma - \rho)D^2} \quad (12)$$

t: Time [min]
η: Coefficient of viscosity of water (=1.00×10^{-2}, 20 °C) [dyne·s/cm^2]
σ: Specific gravity of particle [2.7 Mg/m^3]
ρ: Specific gravity of water [≈1.0 Mg/m^3]
D: Particle diameter [0.5 μm = 5×10^{-5} cm]
R: Distance from the axis of rotation to the bottom surface of settled particles (distance from the center of the rotor to the bottom surface of the centrifuge tube) [cm]
S: Distance from the axis of rotation to the surface of suspension [cm]
N: Number of revolutions [rpm]

In this study, the specifications of the centrifuge (manufactured by AS ONE Corporation, Tokyo, Japan) and centrifuge tube were examined, and t = 219 s (3 min 39 s) was obtained for the condition of R = 15 cm, S = 9 cm, and centrifugation was performed at 3000 rpm for 4 min. The supernatant was discarded and washed with 80% ethyl alcohol

(Junsei Chemical Co., Ltd., Tokyo, Japan, 99.5% purity). This procedure was repeated three times.

To remove residual chloride ion (Cl^-), the washed suspension was filled into a cellulose tube for dialysis (KENIS LIMITED Co., Ltd., Osaka, Japan), tied at both ends, and brought into contact with a large volume of distilled water (3 L) for about 5 days. The pH and conductivity of the distilled water were measured every 24 h using a personal pH/ORP meter (Yokogawa Electric Corp., Tokyo, Japan) and a personal SC meter (Yokogawa Electric Corp., Tokyo, Japan). To confirm the removal of Cl^- ions, the distilled water was changed about every 5 days, and a small amount of the distilled water that had been in contact was separated into test tubes, and several drops of 0.1 M-$AgNO_3$ (Hayashi Pure Chemical Industries, Ltd., Shiga, Japan) were added until no AgCl was observed. During this process, a total of 5 washings with distilled water and precipitation checks of AgCl by $AgNO_3$ were repeated. After AgCl was no longer cloudy, the suspension in the cellulose dialysis tube was transferred to a flat-bottomed container and dehydrated at room temperature. Afterwards, the sample (plate-like) obtained by natural dehydration was crushed in a mortar and dried in a constant-temperature oven at 105 °C to obtain Ca-montmorillonite powder. Although about 10 g of Ca-montmorillonite sample was obtained by the procedure described above, substitutional synthesis to Ca-montmorillonite was carried out twice. Therefore, a total of about 20 g of Ca-montmorillonite sample was obtained (since the recovery of the sample was 95.45%, the sample actually obtained was approximately 19 g).

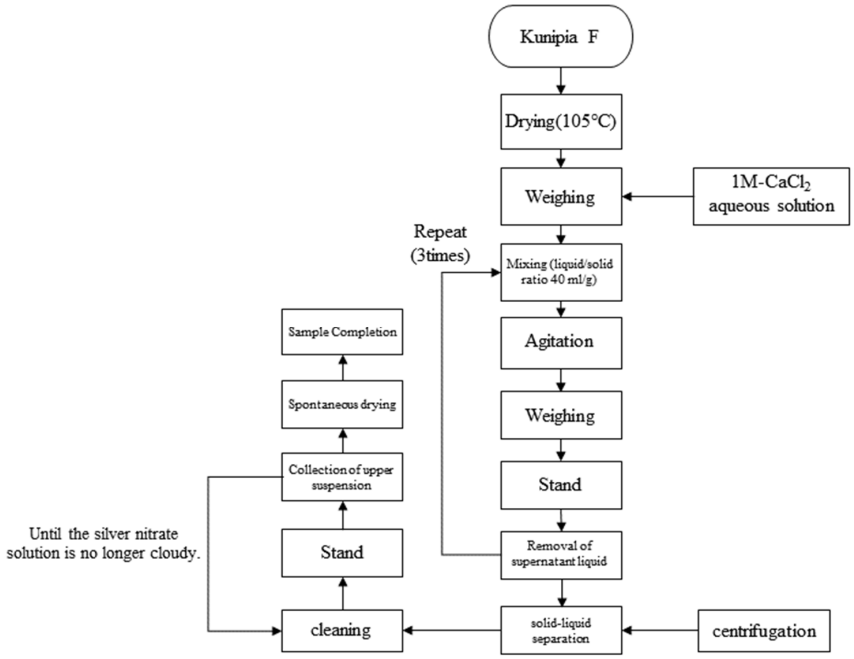

Figure 6. Flowchart of refining of Ca-montmorillonite.

2.3. Measurements of Thermodynamic Data of Water in Ca-Montmorillonite by Relative Humidity (RH) Method

The thermodynamic data of water in the Ca-montmorillonite synthesized in Section 2.2 were measured using the relative humidity method (RHM) [19]. Figure 7 shows a diagram of the Ca-montmorillonite water adsorption experiment. A quantity of 2.00 g of Ca-montmorillonite powder was dried in a thermostatic chamber at 105 °C and then weighed on an electronic balance into three weighing bottles. To allow water vapor to adhere to the samples, the weighing bottles, beakers containing distilled water, and relative humidity/thermometer (manufactured by AND Co., Ltd., Tokyo, Japan) were evacuated using a vacuum desiccator (manufactured by SANPLATEC Co., Ltd., Osaka, Japan) and maintained at 100% in relative humidity and 25 °C. The water content was weighed approximately every 24 h until there was no change in weight, i.e., until saturated.

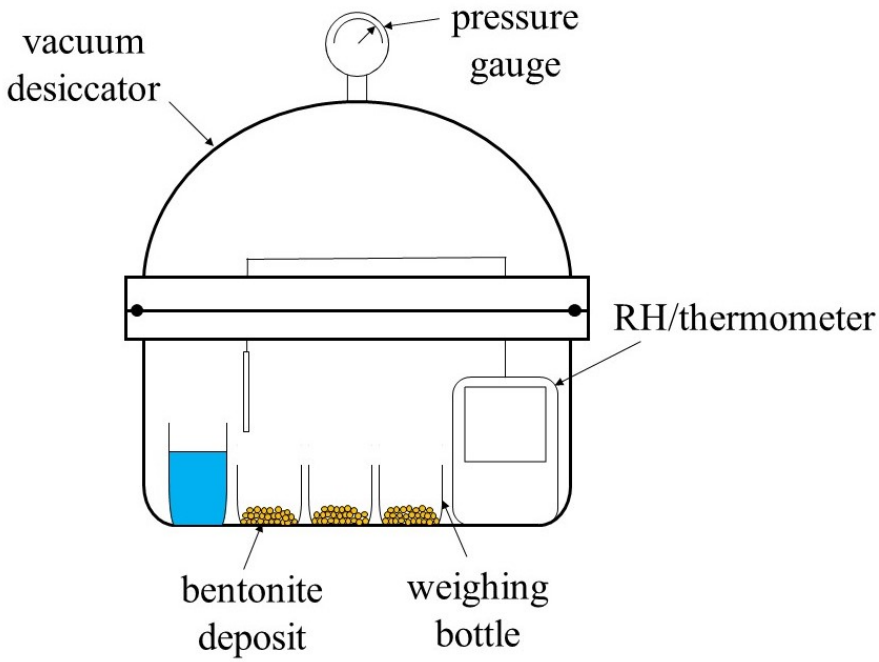

Figure 7. Ca-montmorillonite water adsorption experiment.

After the water adsorption experiments were completed, dehydration experiments were conducted. Figure 8 shows a diagram of the Ca-montmorillonite dehydration experiment. The weighing bottle was removed from the vacuum desiccator, inserted into a sealed acrylic container fitted with a relative humidity/temperature sensor, and placed in a thermostatic chamber (internal temperature 25 °C). After approximately 24 h, the relative humidity and temperature were read from the sensors, and the weighing bottles were removed and weighed for water content. After the weight for water content was measured, vacuuming was performed to lower the water content of the sample for a while, and the weighing bottle was returned to the sealed container. This process was repeated for approximately two months. As described above, in this experiment, relative humidity and temperature were measured as a function of water content.

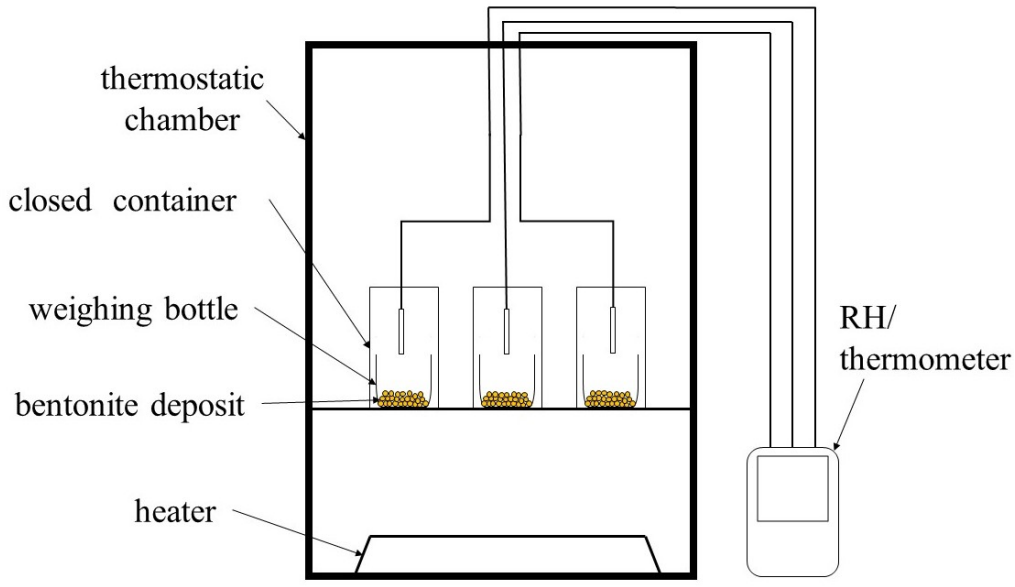

Figure 8. Ca-montmorillonite water dehydration experiment.

3. Experimental Results and Discussion

3.1. The Measurement Results of Thermodynamic Data

Figure 9 shows an example of the moisture adsorption process obtained in the experiment described in Section 2.3.

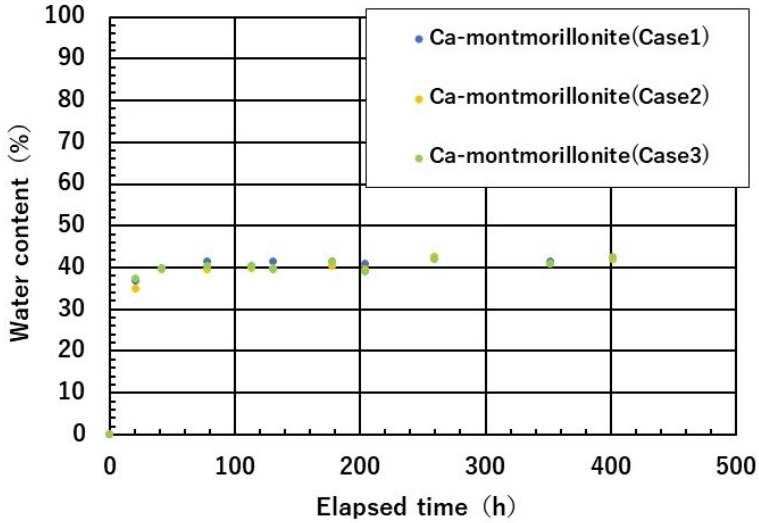

Figure 9. Relationship between elapsed time and water content in water adsorption experiments.

Figure 9 shows a diagram of the water dehydration process obtained in the experiments described in Section 2.3. The water content of Ca-montmorillonite was about 40% after about 40 h, indicating that the montmorillonite was saturated with water in a short time. This corresponds to two-layer hydration (44.8% in water content) from the surface of montmorillonite, which is generally consistent with the results of previous studies [23].

However, as described in previous studies [24], thermodynamic data for Ca-montmorillonite in the single-layer hydration process cannot be obtained because the two-layer hydration process occurs beyond the single-layer hydration process in the hydration process. In this study, therefore, we obtained thermodynamic data during the process of desorbing water from Ca-montmorillonite after being saturated with water, thereby obtaining accurate data. Figure 10 shows data on the water content obtained in the water desorption experiment.

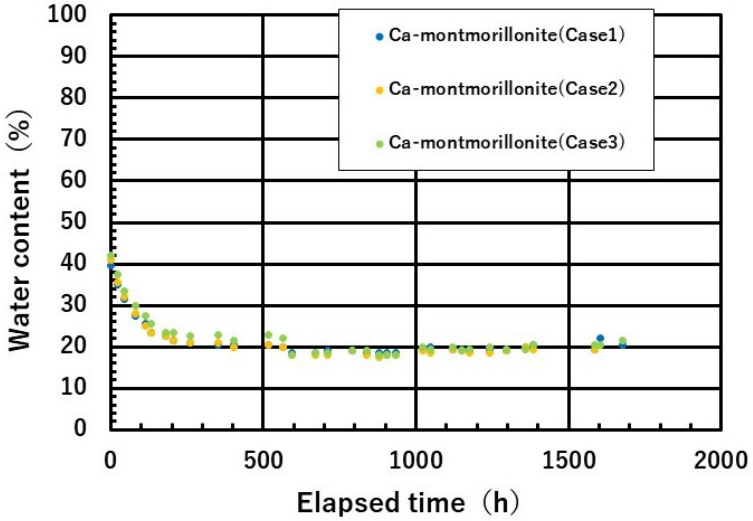

Figure 10. Relationship between elapsed time and water content ratio in water desorption experiments.

Then, from the temperature and relative humidity measured by the relative humidity method, the activity of water (a_{H_2O}) and the relative partial molar Gibbs free energy (dG_{H_2O}) in the β phase (bentonite phase) were obtained based on Equations (2) and (3), and comparisons with Kunipia P (Na-montmorillonite) are shown in Figures 11 and 12, respectively. The water activity and relative partial molar Gibbs free energy began to decrease once the water content fell below 30%. This indicates that the interlayer water affected by the Ca-montmorillonite surface is in the range of two to three water molecules. The relative partial molar Gibbs free energy was about −4 kJ/mol at a water content of about 10%, which is slightly lower than that of Na-montmorillonite. This indicates that the swelling energy of Ca-montmorillonite is higher than that of Na-montmorillonite in the range of high dry density. That is to say, the water activity and the relative partial molar Gibbs free energy of water in Ca-montmorillonite decreased with decreasing water content, indicating that the water near the montmorillonite surface is bound to decreasing water content of montmorillonite. This trend is like that of Kunipia P (100% montmorillonite content), a Na-bentonite that was used for comparison. However, because Ca-montmorillonite has a lower water content than Na-montmorillonite, data on water activity and relative partial molar Gibbs free energy were not obtained for water content above 40%. This is a subject for future work.

Figure 13 shows the relationship between montmorillonite partial density and the relative partial molar Gibbs free energy of water. The relative partial molar Gibbs free energy of water in Ca-montmorillonite decreased with increasing montmorillonite partial density. Similarly, the relative partial molar Gibbs free energy of water in Na-montmorillonite obtained in previous studies [18] also decreases with increasing montmorillonite partial density. Furthermore, Figure 13 shows that the relative partial molar Gibbs free energy of Na-montmorillonite and Ca-montmorillonite coincide in the montmorillonite partial density range of 1.3 Mg/m^3 to 1.8 Mg/m^3.

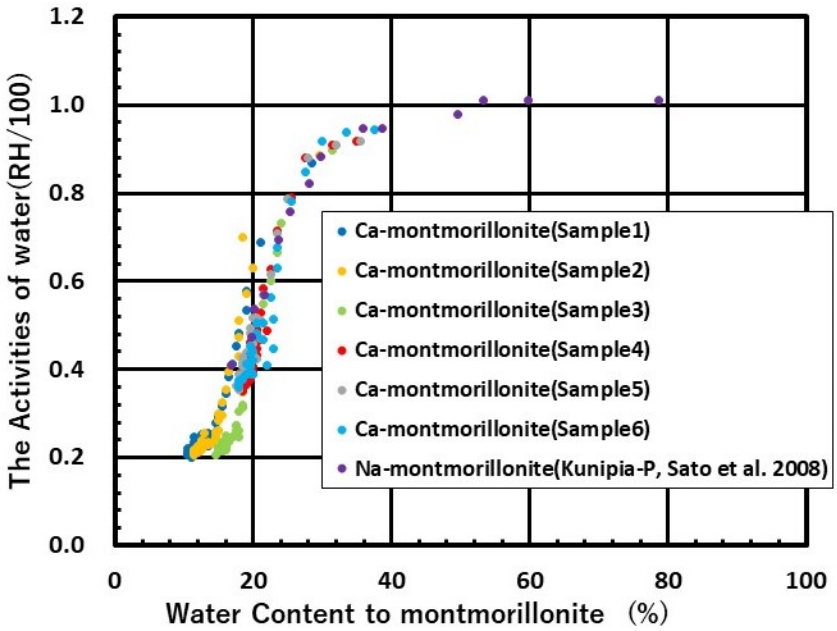

Figure 11. Relationship between water content and water activity [18].

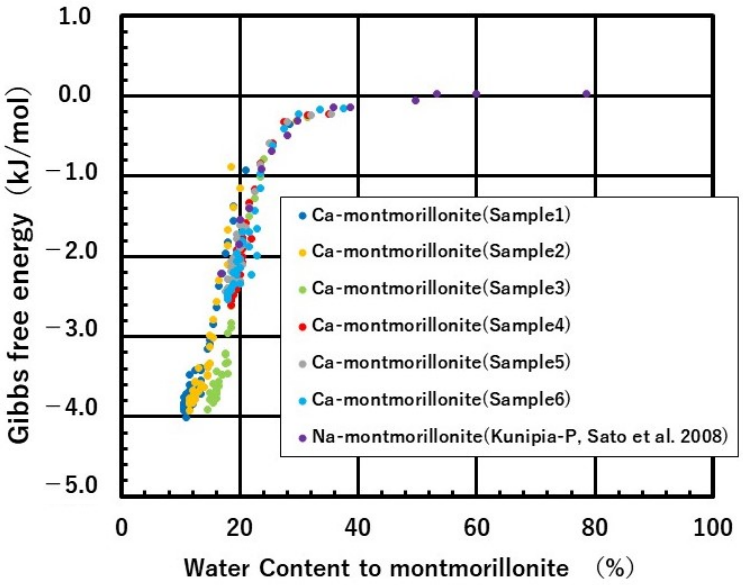

Figure 12. Relationship between water content and relative partial molar Gibbs free energy [18].

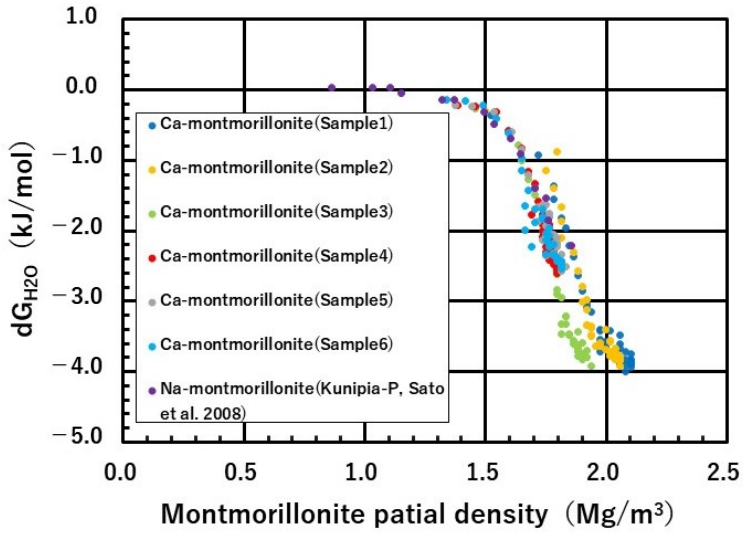

Figure 13. Relationship between montmorillonite partial density and relative partial molar Gibbs free energy [18].

3.2. Comparison of Swelling Stress with Measured Data

Figure 14 compares the measured swelling stress against montmorillonite partial density under pure water conditions for various Na-bentonite and silica sand mixtures with different montmorillonite content, and for Ca-type Kunigel V1 [10,18,25,26], with the swelling stress of Na-montmorillonite and Ca-montmorillonite analyzed by a thermodynamic model. The swelling stress of Ca-montmorillonite (analytical value) was approximately the same level as that of Na-montmorillonite (measured value) in the low-density range of 1.3 Mg/m^3 to 1.7 Mg/m^3 and was higher than that of Na-montmorillonite (measured value) in the high-density range of 1.8 Mg/m^3 to 2.0 Mg/m^3. On the other hand, in such high-density range, the same levels of swelling stress were analyzed based on the same thermodynamic model and the thermodynamic data of interlayer water for Na-montmorillonite (ex., Kunipia P, reported by Sato et al. [18]). Since data variations are also considered, further data acquisition is needed for detailed discussion. The relationship between montmorillonite partial density and swelling stress showed no significant differences among Na-bentonite, Ca-bentonite, and Ca-montmorillonite. However, the

analytical value of swelling stress for Ca-montmorillonite in the low-density region has not been calculated, and further data acquisition is needed for the versatility and practicality of the thermodynamic model. Table 2 shows the thermodynamic data for water in Ca-montmorillonite obtained in the experiments of Section 2.2.

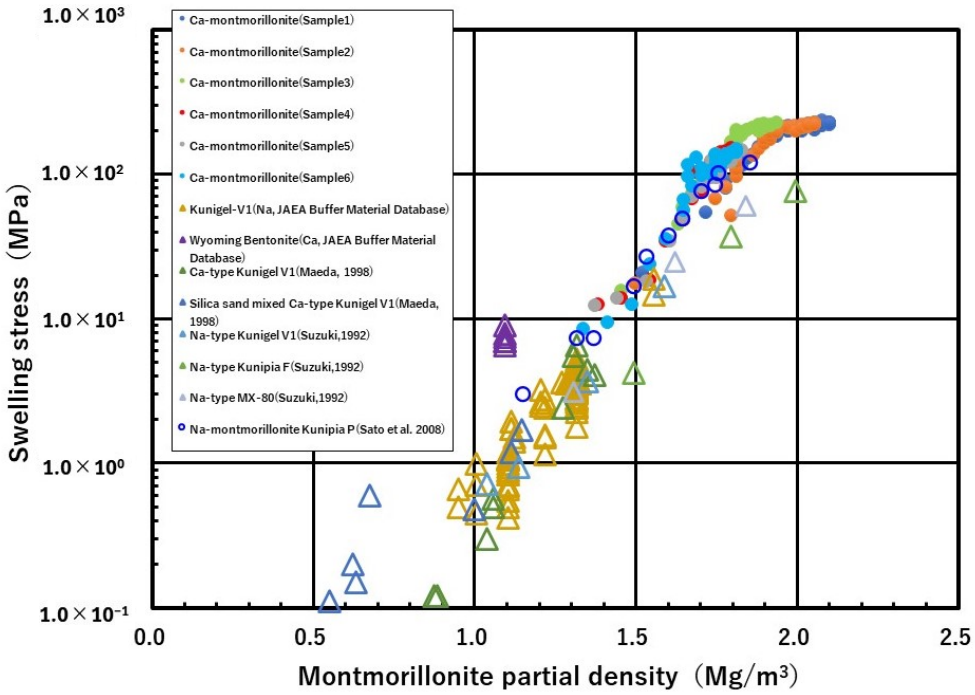

Figure 14. Relationship between montmorillonite partial density and swelling stress [10,18,25,26].

Table 2. Thermodynamic data on water in Ca-montmorillonite obtained from the experiments in Section 2.2.

	Water Content (%)	a_{H_2O}	dG_{H_2O} (J/mol)
Ca-montmorillonite (Sample 1)	28.5	0.867	−0.353906242
	21	0.688	−0.927979537
	19	0.577	−1.36641129
	19	0.535	−1.555759795
	18	0.481	−1.816753027
	17.5	0.454	−1.964750592
	17	0.411	−2.208630293
	16.5	0.384	−2.373437109
	16	0.346	−2.632722863
	15.5	0.317	−2.847958472
	15	0.293	−3.045166027
	15	0.288	−3.094072657
	14.5	0.28	−3.15562721
	13.5	0.252	−3.417957406
	14.5	0.257	−3.371496345
	13.5	0.235	−3.597175071
	13.5	0.225	−3.711390882
	13	0.23	−3.642041621
	12	0.219	−3.76475126
	12	0.213	−3.834901407
	11.5	0.21	−3.884349843
	11.5	0.213	−3.833615606
	11	0.207	−3.907066884
	11	0.199	−4.00483796

Table 2. *Cont.*

	Water Content (%)	a_{H_2O}	dG_{H_2O} (J/mol)
	10.5	0.205	−3.929833132
	10.5	0.211	−3.858295811
	10.5	0.209	−3.883214586
	10.5	0.208	−3.892500964
	11.5	0.227	−3.677043399
	11.5	0.246	−3.478880276
	11.5	0.234	−3.602937122
	11	0.223	−3.721129689
	10.5	0.22	−3.753457586
	11	0.214	−3.822004544
	10.5	0.213	−3.832329805
	12	0.219	−3.766013964
	13.5	0.239	−3.54930073
	13	0.237	−3.570139412
	13.5	0.254	−3.397214801
	12.5	0.252	−3.416811401
Ca-montmorillonite (Sample 2)	29.5	0.885	−0.302949891
	18.5	0.701	−0.880938389
	20	0.629	−1.151231421
	19	0.572	−1.388501448
	18	0.511	−1.665452715
	18	0.472	−1.866760241
	18	0.429	−2.100751875
	16.5	0.395	−2.302627611
	16	0.355	−2.568161912
	15.5	0.324	−2.792876683
	15	0.3	−2.984596847
	15.5	0.297	−3.015567567
	15	0.284	−3.119417501
	15	0.26	−3.339337689
	14.5	0.258	−3.360733189
	13.5	0.236	−3.58542697
	13	0.227	−3.688139255
	13.5	0.23	−3.639597707
	12.5	0.222	−3.729772042
	12.5	0.217	−3.786223813
	12	0.217	−3.801467794
	12.5	0.223	−3.719882034
	11.5	0.212	−3.845281307
	11.5	0.205	−3.928515501
	11.5	0.213	−3.832329805
	11.5	0.215	−3.809169584
	12	0.213	−3.833615606
	12	0.217	−3.784953481
	12.5	0.237	−3.567745353
	13	0.254	−3.397214801
	12.5	0.237	−3.568942382
	12	0.227	−3.674577654
	12	0.221	−3.739704841
	12	0.216	−3.796395968
	11.5	0.218	−3.773563603
	14	0.231	−3.631290517
	14.5	0.246	−3.475382156
	14.5	0.244	−3.495611865
	15	0.26	−3.33709765
	14.5	0.256	−3.376638991

Table 2. *Cont.*

	Water Content (%)	a_{H_2O}	dG_{H_2O} (J/mol)
Ca-montmorillonite (Sample 3)	31.5	0.898	−0.266788566
	24	0.731	−0.777281959
	23.5	0.666	−1.009638503
	22.5	0.6	−1.270137287
	21.5	0.548	−1.492543349
	20.5	0.507	−1.689464922
	20	0.459	−1.933613662
	20	0.424	−2.127712631
	19	0.38	−2.400208212
	18.5	0.347	−2.623803726
	18.5	0.319	−2.834267458
	18.5	0.312	−2.894149386
	18	0.304	−2.951762499
	17.5	0.274	−3.210401543
	17.5	0.273	−3.221627327
	17	0.247	−3.472304896
	16.5	0.234	−3.61380571
	16.5	0.238	−3.557311125
	16	0.226	−3.685518623
	16	0.218	−3.776096621
	15	0.218	−3.791294729
	16	0.224	−3.71003442
	15.5	0.216	−3.800218485
	14.5	0.206	−3.916452426
	15.5	0.214	−3.823286451
	15.5	0.219	−3.76475126
	15.5	0.216	−3.798944313
	15.5	0.216	−3.797670141
	16	0.232	−3.621800612
	16	0.25	−3.436564152
	15.5	0.235	−3.589950619
	16	0.228	−3.664913995
	15	0.224	−3.707546551
	15.5	0.218	−3.776096621
	15.5	0.221	−3.740959987
	16	0.229	−3.65406515
	18	0.247	−3.466491562
	17	0.246	−3.476548196
	17.5	0.261	−3.329821527
	18	0.262	−3.320341757
Ca-montmorillonite (Sample 4)	35	0.917	−0.214868233
	31.5	0.908	−0.239246375
	27.5	0.88	−0.316999721
	25.5	0.789	−0.587485444
	23.5	0.714	−0.834811906
	22.5	0.626	−1.160766186
	21.5	0.584	−1.332870491
	21	0.527	−1.587907652
	20.5	0.489	−1.773427984
	20.5	0.446	−2.002271299
	20.5	0.432	−2.079964379
	20	0.394	−2.30891141
	18.5	0.363	−2.512057166
	18.5	0.371	−2.458017816
	19	0.367	−2.485723678
	19	0.377	−2.421491936
	18.5	0.383	−2.379105359
	18.5	0.359	−2.540376876

Table 2. *Cont.*

	Water Content (%)	a_{H_2O}	dG_{H_2O} (J/mol)
	18.5	0.35	−2.602463935
	18.5	0.358	−2.549002164
	19.5	0.378	−2.414107467
	20	0.407	−2.228438822
	19.5	0.428	−2.103722469
	19.5	0.407	−2.229186244
	19	0.397	−2.289339494
	19.5	0.41	−2.210233425
	19	0.424	−2.12842603
	20	0.435	−2.06419886
	20.5	0.463	−1.909507118
	19.5	0.462	−1.914868825
	22	0.489	−1.774022795
	20.5	0.49	−1.768956831
Ca-montmorillonite (Sample 5)	35.5	0.918	−0.219563691
	32	0.909	−0.242070739
	28	0.881	−0.317238306
	25	0.788	−0.590629334
	23.5	0.709	−0.848223696
	22.5	0.615	−1.194998008
	21.5	0.568	−1.385721738
	21	0.512	−1.637226001
	21	0.47	−1.846558115
	20	0.435	−2.028901579
	20.5	0.423	−2.10066143
	20	0.388	−2.307593833
	18	0.36	−2.473168174
	18	0.371	−2.400308191
	18	0.371	−2.400308191
	19	0.389	−2.293469679
	18	0.389	−2.285619363
	17.5	0.364	−2.442217915
	18	0.355	−2.50702545
	18	0.367	−2.426549703
	19	0.393	−2.268619639
	18.5	0.415	−2.132654645
	19.5	0.442	−1.98659738
	19	0.415	−2.136310834
	18.5	0.407	−2.179856389
	18.5	0.428	−2.05785899
	19	0.437	−2.010837999
	20	0.459	−1.898003834
	19.5	0.482	−1.775796585
	19.5	0.494	−1.715960107
	20	0.517	−1.607972932
	20.5	0.517	−1.610715509
Ca-montmorillonite (Sample 6)	37.5	0.943	−0.1454875
	33.5	0.937	−0.161310683
	30	0.917	−0.214796189
	27.5	0.849	−0.405659474
	25.5	0.781	−0.6125434
	23.5	0.677	−0.966352819
	23.5	0.629	−1.14853307
	22.5	0.562	−1.428028362
	23	0.514	−1.64982526
	21.5	0.468	−1.8822398
	23	0.448	−1.988505546
	22	0.408	−2.222355484

Table 2. *Cont.*

Water Content (%)	a_{H_2O}	dG_{H_2O} (J/mol)
18	0.375	−2.431433566
18.5	0.381	−2.390479598
18.5	0.376	−2.425645105
19	0.388	−2.349313927
19	0.389	−2.340571567
18	0.366	−2.491654107
18	0.359	−2.53952511
18	0.367	−2.486557109
20	0.39	−2.335772898
19.5	0.416	−2.173489647
20	0.44	−2.034492905
19	0.411	−2.203455255
19.5	0.407	−2.226943973
20	0.422	−2.138002755
19.5	0.435	−2.063506752
19.5	0.453	−1.962994727
20.5	0.476	−1.840839787
20.5	0.483	−1.804032777
20.5	0.504	−1.698529322
21.5	0.505	−1.693047588

4. Conclusions

4.1. Summary

In this study, thermodynamic data on Ca-montmorillonite were obtained as a function of water content by measuring relative humidity (RH) and temperature. The activities of water and the relative partial molar Gibbs free energies of water were determined from the experimental results, and the swelling stress of Ca-bentonite was calculated using the thermodynamic model and compared with measured data.

Ca-montmorillonite was obtained by replacing all interlayer cations (mainly Na) of Kunipia F (99% Na-montmorillonite content) with Ca and removing soluble salts beforehand. The activities of water and the relative partial molar Gibbs free energies obtained in the experiments decreased with decreasing water content in water contents lower than about 25%. This trend was similar to that of Na-montmorillonite. The relationship between water activity and the relative partial molar Gibbs free energy and water content indicates that Ca-montmorillonite has a similar degree of water binding near the montmorillonite surface compared to Na-montmorillonite. The relationship between montmorillonite partial density and relative partial molar Gibbs free energy also indicates that the degree of surface binding is comparable.

The swelling stress calculated based on the thermodynamic model was approximately 200 MPa at a montmorillonite partial density of 2.0 Mg/m^3, and approximately 10 MPa at a montmorillonite partial density of 1.4 Mg/m^3. The swelling stresses in the high-density region were higher than that of Na-montmorillonite and were similar levels in the low-density region. Comparison with measured data showed the practicality of the thermodynamic model. Ca-montmorillonite showed the same swelling stress as that of Na-montmorillonite in the low-density region. Furthermore, in the high-density region, the swelling stress was higher than that of Na-montmorillonite (measured value). This indicates that setting the montmorillonite partial density in the high-density region in the design conditions of the buffer material may break the pressure equilibrium in the surrounding host rock (natural barrier) when the Na-montmorillonite is converted to Ca-montmorillonite. In the low-density region, the results are consistent with existing measured data, indicating the practicality and versatility of the thermodynamic model.

4.2. Future Works

In this study, we obtained thermodynamic data of water in Ca-montmorillonite by the relative humidity method, calculated analytical values of swelling stress, and compared them with measured values. However, the thermodynamic data of water in Ca-montmorillonite obtained this time are still insufficient. Therefore, we believe it is necessary to continue to acquire more precise data in the future. In this experiment, the temperature was fixed at 25 °C. However, in an actual disposal environment, the temperature may change due to the decay heat in the vitrified waste. Since the function of the buffer material may change as the temperature changes, we plan to conduct experiments at different temperatures. We believe it is necessary to demonstrate the versatility and practicality of the thermodynamic model by using more precise thermodynamic data to compare analytical values with measured values.

Author Contributions: Conceptualization, K.I. and H.S.; methodology, K.I. and H.S.; validation, K.I. and H.S.; formal analysis, K.I.; investigation, K.I. and H.S.; resources, K.I. and H.S; data curation, K.I.; writing—original draft preparation, K.I.; writing—review and editing, K.I. and H.S.; visualization, K.I.; supervision, H.S.; project administration, K.I. and H.S.; funding acquisition, H.S. All authors have read and agreed to the published version of the manuscript.

Funding: This work was supported by JSPS KAKENHI Grant Number JP20K05383.

Data Availability Statement: Dataset available on request from the authors; The raw data supportingthe conclusions of this article will be made available by the authors on request.

Conflicts of Interest: The authors declare no conflicts of interest.

References

1. Tochiyama, O. Radioactive Waste Management Funding and Research Center: Principles and Basis of Radioactive Waste Disposal. Available online: https://www.rwmc.or.jp/library/file/RWMC_GensokuKiso_170809.pdf (accessed on 27 January 2024).
2. Onikata, M. Characteristics and Application of Bentonite. *Clay Sci.* **2007**, *46*, 131–138. [CrossRef]
3. Sato, H. Function for Controlling Nuclide Migration of Buffer Material in the Geological Disposal for High-Level Radioactive Waste. *J. MMIJ* **2009**, *125*, 1–12. [CrossRef]
4. Sato, H. Swelling of Buffer Material as an Engineered Barrier in Geological Disposal and Its Thermodynamics. *Genshiryoku Bakkuendo Kenkyu* **2020**, *27*, 105–114. Available online: https://nuce.aesj.or.jp/jnuce/vol27/Jnuce-Vol27-2-p105-114.pdf (accessed on 16 February 2024).
5. Japan Nuclear Cycle Development Institute. *Technical Reliability of Geological Disposal of High-Level Radioactive Waste in Japan—Second Progress Report on Research and Development of Geological Disposal—General Report*; JNC TN1400 99-020; Japan Nuclear Cycle Development Institute: Ibaraki, Japan, 1999. (In Japanese)
6. Nuclear Waste Management Organization of Japan. Realization of Safe Geological Disposal in Japan—Building a Safety Case for Appropriate Site Selection. NUMO-TR-20-03. 2021. Available online: https://www.numo.or.jp/technology/technical_report/tr180203.html (accessed on 21 April 2024).
7. Horonobe Underground Research Unit; Geological Isolation Research and Development Directorate. *Horonobe Underground Research Laboratory Project Synthesis of Phase I Investigations 2001–2005 Volume "Geoscientific Research"*; JAEA-Research 2007-044; Japan Atomic Energy Agency: Ibaraki, Japan, 2007.
8. Niunoya, S.; Matsui, H. *The Investigation on Rock Mechanics in HDB-1 and HDB-2 Boreholes in Order to Select URL Area*; JNC TN5400 2005-012; Japan Nuclear Cycle Development Institute: Ibaraki, Japan, 2005.
9. Power Reactor and Nuclear Fuel Development Corporation. *Technical Report on Research and Development of Geological Disposal of High-Level Radioactive Waste*; PNC TN1410 92-081; Power Reactor and Nuclear Fuel Development Corporation: Ibaraki, Japan, 1992.
10. Maeda, M.; Tanai, K.; Ito, M.; Mihara, M.; Tanaka, M. *Mechanical Properties of the Ca Exchanged Ca Bentonite—Swelling Pressure, Hydraulic Conductivity, Compressive Strength and Elastic Modulus*; PNC TN8410 98-021; Power Reactor and Nuclear Fuel Development Corporation: Ibaraki, Japan, 1998.
11. Kubo, H.; Kuroki, Y.; Mihara, M. Experimental Investigation on Alteration of Bentonite by Concrete Pore Fluids. *Tsuchi Kiso* **1998**, *46*, 31–34.
12. Sagawa, O.; Hyodo, A.; Nakata, Y.; Yoshimoto, N.; Fujiwara, A. Influence of the Ca Substitution for Mechanical Characteristics of Na-Type Bentonite and Sand Mixture for Long Term Seapage. *Civ. Eng. Soc. Proc.* **2008**, *64*, 43–56. [CrossRef]
13. Kurosawa, S.; Shibata, M.; Ueta, S.; Ichige, S.; Hayashi, K.; Yui, M. Alternation of Bentonite in Highly Alkaline Conditions and Its Effect on Colloid Filtration. *Jpn. At. Energy Soc. J. Lit.* **2002**, *1*, 244–248. [CrossRef]

14. Savage, D.; Bateman, K.; Hill, P.; Hughes, C.; Milodowski, A.; Pearce, J.; Rae, E.; Rochelle, C. Rate and mechanism of the reaction of silicates with cement pore fluids. *Appl. Clay Sci.* **1992**, *7*, 33–45. [CrossRef]
15. Gahr, G.; Bucher, F.; Mayor, P.A. Water Uptake and Swelling Pressure in a Bentonite-Based Backfill. *Mater. Res. Soc. Symp. Proc.* **1988**, *127*, 683–689. [CrossRef]
16. Kanno, T.; Wakamatsu, H. Moisture Adsorption and Volume Change of Partially Saturated Bentonite Buffer Materials. *Mater. Res. Soc. Symp. Proc.* **1992**, *294*, 425–430. [CrossRef]
17. Torikai, Y. Study on Characterization of Water in Geological Disposal Engineering Barrier Materials Bentonite. Ph.D. Thesis, Hokkaido University Graduate School of Engineering, Hokkaido, Japan, 1996.
18. Sato, H. A Thermodynamic Approach Effect of Salinity on Swelling Pressure of Bentonite. In Proceedings of the 4th Japan-Korea Joint Workshop on Radioactive Waste Disposal 2008: Perspective of Science and Engineering, Hakone, Japan, 27–28 May 2008.
19. Sato, H. Measurements of Thermodynamic Data of Water in Na-Bentonite in the Pressure Release System and Standard Condition by Relative Humidity Method. In Proceedings of the AESJ2022 Fall Meeting 3C12, Hitachi, Japan, 7–9 September 2022.
20. Sato, H.; Miyamoto, S. *A Study on Diffusion and Migration of Lead in Compacted Bentonite*; JNC Tech. Rep. JNC TN8400 2001-018; JNC Tokai: Ibaraki-Ken, Japan, 2001.
21. Sato, H. *Purification of Na-Smectite and Preparation of Oriented Samples for Diffusion Experiments*; JAEA-Research 2005-004; Japan Atomic Energy Agency: Ibaraki, Japan, 2005.
22. Sato, H.; Ashida, T.; Kohara, Y.; Yui, M.; Sasaki, N. Effect of Dry Density on Diffusion of Some Radionuclides in Compacted Sodium Bentonite. *J. Nucl. Sci. Technol.* **1992**, *29*, 873–882. [CrossRef]
23. Sato, H. Thrmodynamic Understanding on Swelling Pressure of Bentonite Buffer. In Proceedings of the 15th International Conference on Nuclear Engineering, Nagoya, Japan, 22–26 April 2007. Paper No. ICONE15-10207.
24. Saito, Y.; Okawara, M. Study on State of Water in Homo-Ionic Montmorillonite by X-Ray Diffraction and Near-Infrared Spectroscopy. *Clay Sci.* **2019**, *58*, 43–59. [CrossRef]
25. Suzuki, H.; Shibata, M.; Yamagata, J.; Hirose, I.; Terakado, K.; Sasaki, N.; Ishikawa, H. *Testing of Buffer Material Properties (I)*; PNC TN8410 92-057; Power Reactor and Nuclear Fuel Development Corporation: Ibaraki, Japan, 1992.
26. Japan Atomic Energy Agency. Buffer Material Database. Available online: https://bufferdb.jaea.go.jp/bmdb/ (accessed on 27 January 2024).